Supplementary Materials

Triboiontronic logic control via dynamic regulation of electrical double layers

Xiang Li[1], Carita Kvarnström[2,*], Ari Ivaska[3,*], Di Wei[1,*]

[1]Beijing Institute of Nanoenergy and Nanosystems, Chinese Academy of Sciences, Beijing 101400, China.

[2]Department of Chemistry, University of Turku, Turku 20014, Finland.

[3]Laboratory of Molecular Science and Engineering, Åbo Akademi University, Turku 20500, Finland.

[*]**Correspondence to:** Prof. Carita Kvarnström, Department of Chemistry, University of Turku, Turku 20014, Finland. E-mail: carkva@utu.fi; Ari Ivaska, Laboratory of Molecular Science and Engineering, Åbo Akademi University, Turku 20500, Finland. E-mail: ari.ivaska@abo.fi; Di Wei, Beijing Institute of Nanoenergy and Nanosystems, Chinese Academy of Sciences, Beijing 101400, China. E-mail: weidi@binn.cas.cn

ORCID: Carita Kvarnström (0000-0002-8734-2294), Ari Ivaska (0000-0002-9534-4871), Di Wei (0000-0003-2670-6362)

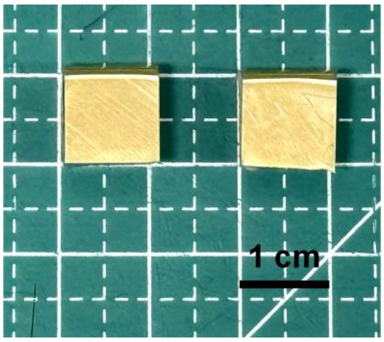

Supplementary Figure 1. The photograph of the TING device.

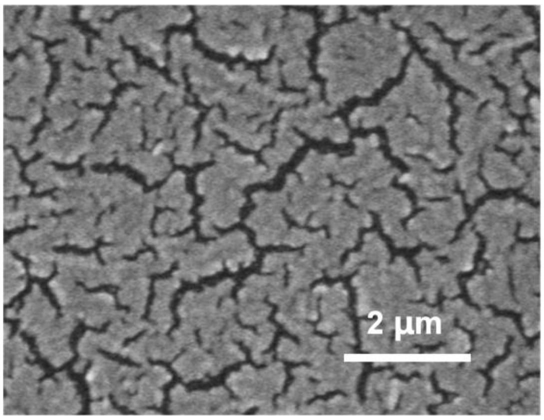

Supplementary Figure 2. The sputtered Au layer of Au/FEP hybrid film contained abundant microscale crack-like structures.

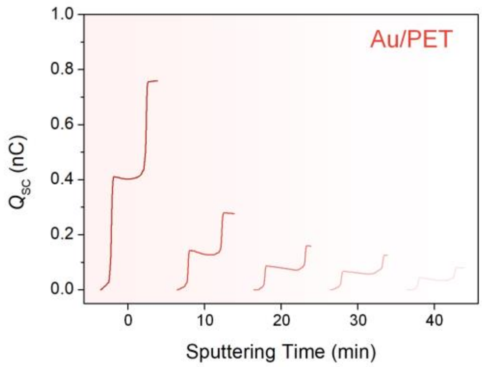

Supplementary Figure 3. Influence of Au sputtering time in metal/dielectric hybrid materials on the Q_{SC} generated by sliding droplets.

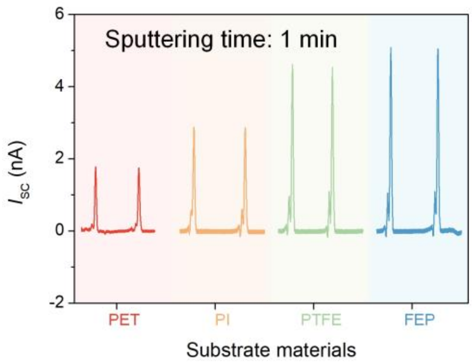

Supplementary Figure 4. Influence of dielectric substrate electronegativity in hybrid materials on the I_{SC} generated by sliding droplets.

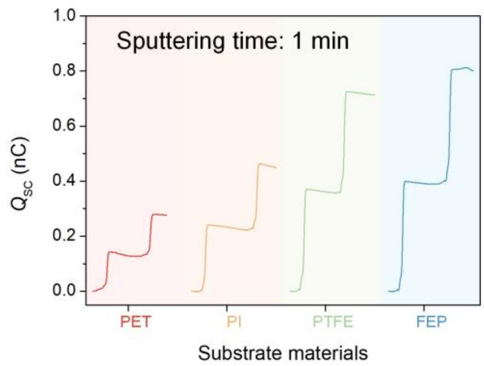

Supplementary Figure 5. Influence of dielectric substrate electronegativity in hybrid materials on the Q_{SC} generated by sliding droplets.

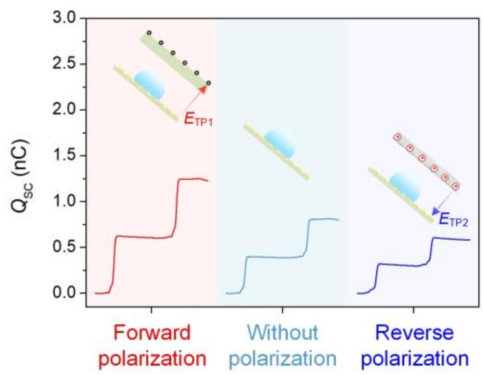

Supplementary Figure 6. Influence of forward and reverse triboelectrically induced ion polarization on the Q_{SC} generated by sliding droplets.

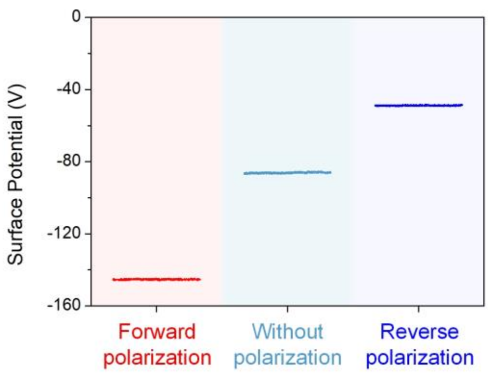

Supplementary Figure 7. Influence of forward and reverse triboelectrically induced ion polarization on the surface potential of Au/FEP hybrid films.

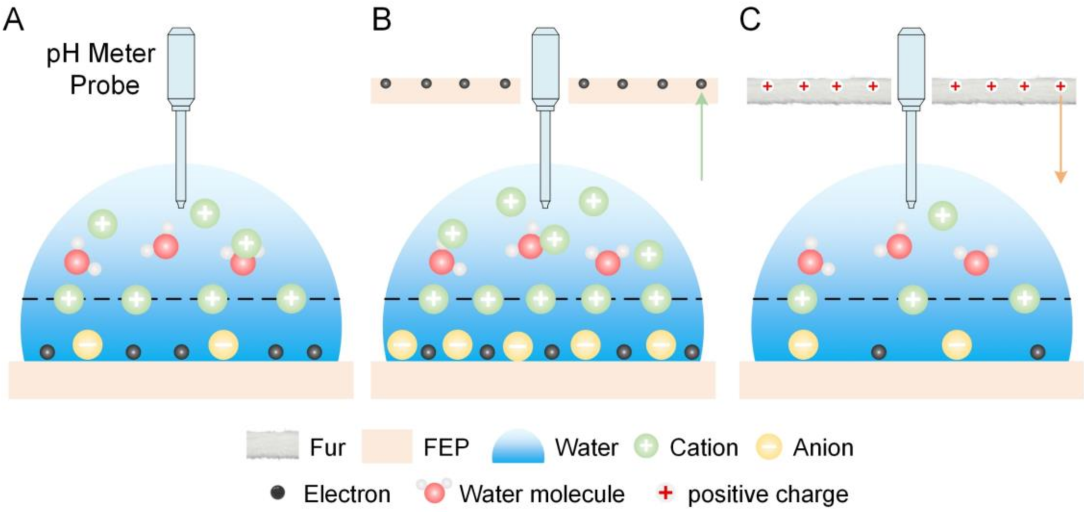

Supplementary Figure 8. Local pH measurement setup under different polarization states at the FEP-water interface. A: Schematic and photograph of the local pH sensing system at the FEP-water interface under the pristine condition without external polarization; B: Local pH measurement under forward polarization, induced by a negatively charged dielectric layer positioned above the liquid; C: Local pH measurement under reverse polarization, induced by a positively charged dielectric layer positioned above the liquid.

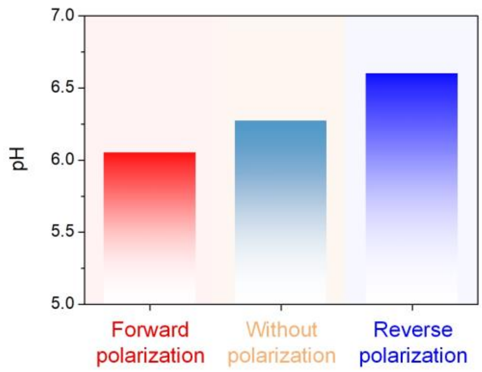

Supplementary Figure 9. Local pH measurements at the FEP-water interface. Under the pristine condition without polarization, the average local pH was measured to be ~6.26. Upon the application of forward polarization, the average pH decreased to ~6.03. In contrast, reverse polarization led to an increase in the average pH to ~6.59.

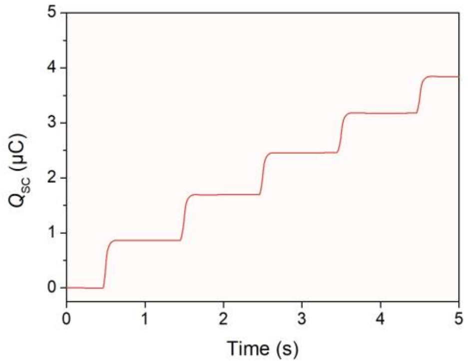

Supplementary Figure 10. Q_{SC} generated by the TING constructed using Au/FEP hybrid films with an Au sputtering time of 1 min.

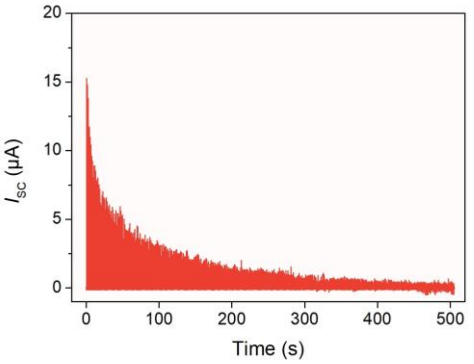

Supplementary Figure 11. After approximately 500 operation cycles, the DC output component became significantly weakened, and AC signals dominated by electrostatic induction gradually appeared.

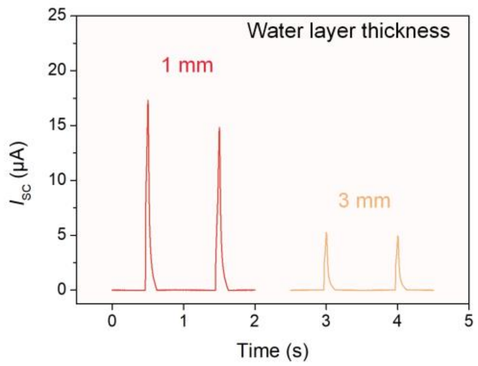

Supplementary Figure 12. The effect of water film thickness on the I_{SC} generated by the TING.

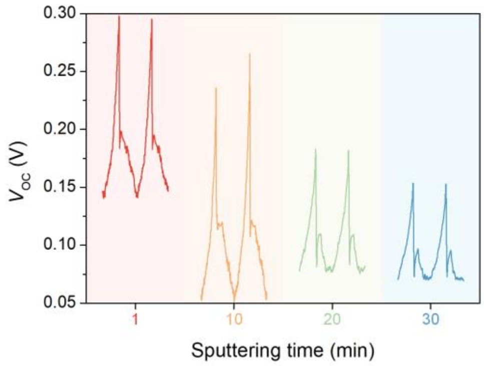

Supplementary Figure 13. The influence of Au sputtering time within the Au/FEP hybrid films on the V_{OC} generated by the TING.

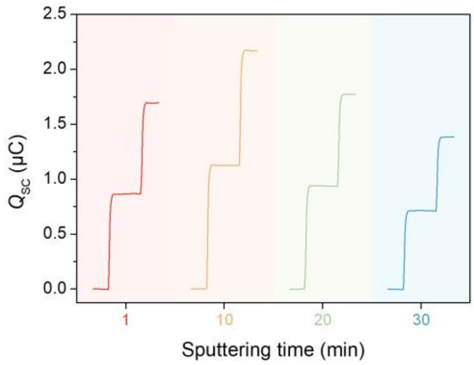

Supplementary Figure 14. Influence of Au sputtering time in Au/FEP hybrid films on the Q_{SC} generated by the TING.

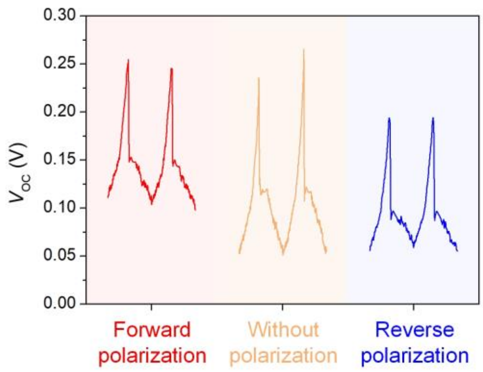

Supplementary Figure 15. Influence of forward and reverse triboelectrically induced ion polarization on the V_{OC} generated by the TING.

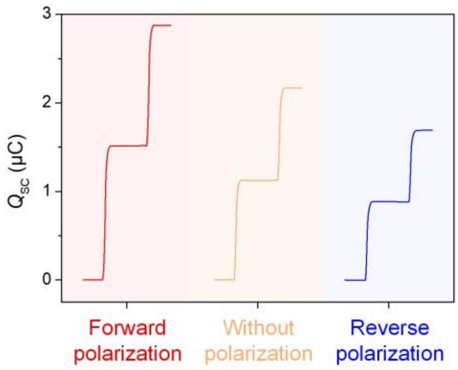

Supplementary Figure 16. Influence of forward and reverse triboelectrically induced ion polarization on the Q_{SC} generated by the TING.

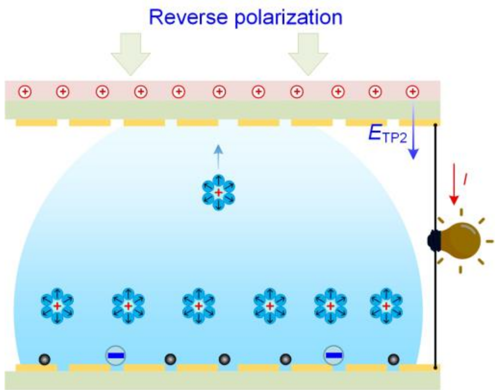

Supplementary Figure 17. Schematic illustration of the reverse triboelectrically induced ion polarization mechanism for reducing ionic migration and ionic-electronic coupling within the TING.

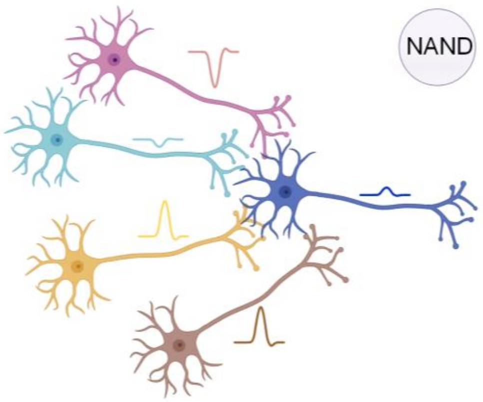

Supplementary Figure 18. Schematic illustration of biological neural signal integration behaviors, where excitatory and inhibitory synaptic coupling enables logic-like computational functions analogous to NAND operations (Created in BioRender. Li, X. (2026) https://BioRender.com/dl2vb37).

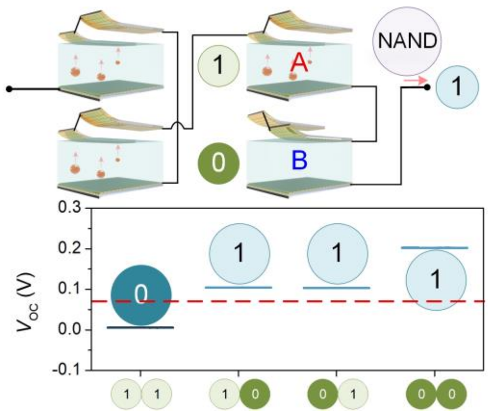

Supplementary Figure 19. Triboiontronic NAND logic gate operations realized using coupled TING units as programmable ionic logic nodes “A” and “B”.